Fast & accurate interatomic potentials for describing thermal vibrations

Andrew Rohskopf[a], Spencer Wyant[a], Kiarash Gordiz[a], Hamid Reza Seyf[b,c],
Murali Gopal Muraleedharan[d], Asegun Henry[a]

[a] *Massachusetts Institute of Technology, Department of Mechanical Engineering, Cambridge, MA 02139, USA*
[b] *School of Mechanical Engineering, Purdue University, West Lafayette, IN 47907, USA*
[c] *George W. Woodruff School of Mechanical Engineering, Georgia Institute of Technology, Atlanta, GA, USA*
[d] *Department of Mechanical Engineering, Pennsylvania State University, University Park, PA 16802, USA*

A B S T R A C T

Molecular dynamics (MD) is a powerful technique that can be used to study thermal vibrations/phonons and properly account for their role in different phenomena that are important in mechanical engineering, chemistry, physics and materials science. However, despite the widespread usage of MD to study various phenomena, direct comparisons between experiments and simulations are often associated with low fidelity, due to the inaccuracy of the interatomic potentials (IAPs) employed. This issue has become the main barrier to utilizing MD for studying phenomena that depend on or involve atomic vibrations, and subsequently deriving physically meaningful insights. Towards solving this problem, we present a new approach to making IAPs that are specifically optimized to accurately describe thermal vibrations/phonons. The approach enables nearly exact reproduction of *ab initio* phonon dispersion relations (i.e., < 1%) error), accurate forces and thermal conductivity (i.e., < 5% and < 10% error respectively), and low computational expense like that of traditional IAPs.

1. Introduction

In solids and molecules, atoms vibrate about their respective equilibrium positions, and this thermal motion can be understood as a superposition of the structure's normal modes, which are usually termed phonons. These vibrations play an important role in a variety of material properties and physical phenomena such as chemical reactions, mass/ion diffusivity, crack propagation, thermal conductivity, electrical conductivity, etc. Thus, it is important that such vibrations can be accurately modeled, so that the modeling of these properties/phenomena is enabled with high fidelity predictive power. Such predictive power is important to realize deeper scientific understanding and enable subsequent efforts to exploit this knowledge towards engineering objectives.

To appreciate the importance of modelling atomic vibrations, consider the growing number of anomalous or unexplained experimental phonon transport results that have persisted in the literature for more than a decade. One example of this was the very low thermal conductivity measured in W/Al_2O_3 laminate structures [1], which was lower than that of fully amorphous Al_2O_3, and its minimum thermal conductivity prediction. Another example is the lower bound of interface conductance in silicon–germanium superlattices according to the diffuse-mismatch model, which was surpassed experimentally. [2] The fact that theoretical calculations for these limiting cases were not able to bound the measurements left many open questions as to how such low thermal conductivity/conductance can be possible. Another interesting case was the measurements of the thermal conductivity of rough silicon nanowires, which reached about the same value as amorphous silicon, but with a clearly crystalline core that was much thicker than

the rough region [3]. More unexplained phenomena include the observation of extremely low thermal conductivity in layered materials [4,5], by Cahill *et al.*, and the lower limit of thermal conductivity in disordered crystals [6] and amorphous materials [7]. In addition to phonon transport, phonon/normal modes also affect chemical reactions, [8] mass/ion diffusion [9], and phase changes [10], and such processes are influenced by exciting specific modes. [11–17] Here it is important to highlight that all of the aforementioned observations lack rigorous theoretical explanations, thus preventing the rational engineering of such effects. As a result, solving the problem of describing thermal vibrations accurately with an IAP that can be evaluated quickly (i.e., fast) will have an impact that spans across multiple disciplines.

In theory, a MD based method such as Green-Kubo modal analysis (GKMA) [18] or interface conductance modal analysis (ICMA) [19] could elucidate what happens in these material systems/measurements, but such a study could be easily dismissed because there isn't an accurate IAP one can use. Thus, the critical problem that must be solved is to develop fast yet accurate IAPs that are constructed purely from *ab initio* inputs, thereby imparting them with high fidelity predictive power. It is from this perspective that we seek to develop a fast, accurate, closed form description of the potential energy surface (PES), so that we can calculate the forces on atoms and the resulting dynamics. First principles methods like density functional theory (DFT) provide an accurate way of probing the PES and predicting atomic forces but are computationally limited to small systems (< 500 atoms) because of the cubic scaling with the number of electrons in the system. Classical methods, however, calculate forces as the spatial gradient of a closed form expression, an analytical IAP, that approximates the PES. Evaluating an IAP computationally scales linearly with the number of atoms
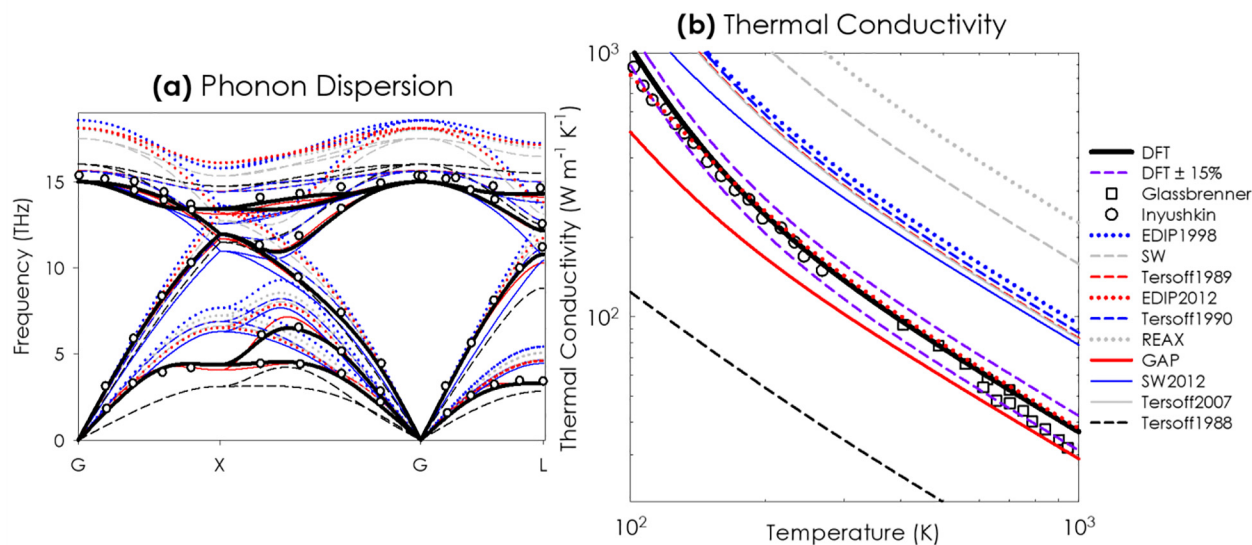
Fig. 1. (a) Phonon dispersion calculated using 10 commonly cited IAPs in literature compared to our DFT calculations (black line), and experiments from literature (circles). (b) Thermal conductivity calculated using the Boltzmann transport equation (BTE) with relaxation time approximation (RTA) for the same 10 potentials compared to our DFT calculations (black line), and experiments from literature (circles and squares). The purple dashed line represents +/- 15% error with respect to DFT, showing that many potentials fall far outside this range. See SI for all calculation details. (For interpretation of the references to colour in this figure legend, the reader is referred to the web version of this article.)

and can therefore be orders of magnitude cheaper to evaluate as compared to DFT. This allows for MD simulations at the relevant length (i.e., 10^3-10^9 atoms) [20] and time (i.e., > 1 ns) [21] scales needed to study vibrational phenomena in a variety of fields such as defect and dislocation dynamics [22], catalysis [23], ion diffusion [24], protein folding [25], and mechanics of materials [26,27].

The problem is that many IAPs are inaccurate, even when just describing thermal vibrations around equilibrium. Fig. 1 for example, shows the dispersion for crystalline silicon (c-Si), calculated with 10 commonly cited IAPs in literature [28–37], compared to our DFT calculations (see supplementary information (SI) for details) and experiments from literature [38].

The thermal conductivity results in Fig. 1 were obtained with the Boltzmann transport equation (BTE) under the relaxation time approximation (RTA) using the Alamode program [39], and only third order force constants were used in computing relaxation times. We note that this suggests our high temperature results are overestimated, since we excluded 4th order force constants in calculating relaxation times, and Feng et al showed that quartic scattering decreases thermal conductivity at high temperatures. [40] However, since our main purpose here is comparing the IAP thermal conductivity to DFT, more computationally expensive full BTE solutions or inclusion of quartic scattering is not needed.

Although the machine learned Gaussian approximation potential (GAP) produces decent agreement on the dispersion, due to its longer-ranged non-radial interaction terms, there is still some discrepancy near the Brillouin zone boundaries because the cutoff radius is not long enough to include all the interactions necessary (i.e., interactions in crystalline silicon need to extend out to 8th nearest neighbors to properly reproduce the dispersion). Nonetheless, such a potential reasonably models thermal conductivity, but the computational cost is the tradeoff, as GAP is currently one of the most computationally expensive potentials with an evaluation time (i.e., on our high performance computing (HPC) hardware) of 0.01 s per timestep per atom per core, [37] which is ~ 1000 times slower than the Tersoff potential. Alternatively, the EDIP parameterization of 2012, [35] which is 3 orders of magnitude faster, exhibits excellent agreement in Fig. 1 for the thermal conductivity, well within 10% over a large range of temperatures. However, it does so for the wrong reasons, because the forces predicted

by this potential deviate by an average of 48% compared to the forces in 50 DFT structures where the atoms are displaced randomly up to 0.05 Å. EDIP 2012 [35] consequently fails to reproduce the vibration dynamics in c-Si, since a force discrepancy around 50% is quite drastic [41], which is further exemplified by its poor description of the harmonic portion of the PES, resulting in significant errors in the phonon dispersion. EDIP 2012 therefore does not accurately model the underlying physics and mode interactions behind thermal transport and as a result, such a potential cannot provide predictive insights for thermal transport or other phenomena that depend on/involve thermal vibrations.

Regarding other machine learned potentials in literature, Minamitani et al obtained excellent phonon dispersion and thermal conductivity agreement for silicon and GaN using neural network potentials. [42] Babaei et al used the GAP potential to obtain excellent phonon dispersion and thermal conductivity for silicon, while also accurately reproducing phonon-vacancy scattering phenomena. [43] Li et al showed excellent agreement for thermal transport in different phases of silicon. [44] All of these recent approaches encompass the traditional machine learning approach, where some function (e.g. neural network, GAP, etc.) are trained to the total force with no post hoc correction of the force. Two methods presented in this manuscript, however, involve a post hoc correction of the harmonic force component and a procedure to machine learn the *anharmonic* force, while modelling the harmonic force separately.

How well an IAP describes thermal vibrations, i.e., the normal modes and their interactions, depends on how well it captures the harmonic and anharmonic aspects of the PES respectively. [45] The harmonic portion of the PES dictates the individual mode characteristics such as mode frequencies/density of states, specific heat, entropy, as well as the mode shapes or dispersion in a material with symmetry. Anharmonicity, on the other hand, determines the mode–mode interactions, that govern phenomena like thermal expansion [46] thermal conductivity [47] joule heating [48], and coupling effects for coherent excitation [49]. The reason it is useful to think about the PES as composed of portions from these two delineations is specifically because the range of interactions that must be included for each portion is usually quite different. More specifically, it is well known that in order to capture the phonon dispersion properly, many materials require
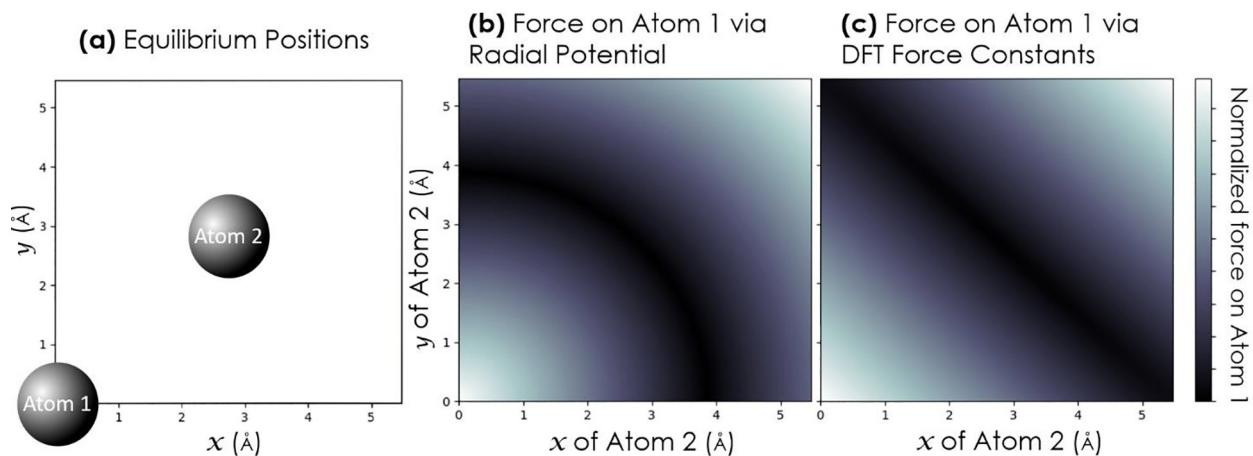
Fig. 2. (a) Equilibrium positions of two atoms (Atom 1 and Atom 2) in the [0 0 1] plane of crystalline silicon (c-Si) as a model example of how radial potentials fail to properly capture interatomic forces. (b) Force magnitude on Atom 1 as Atom 2 is moved in the [0 0 1] plane, calculated via a radial Morse potential. (c) Force magnitude on Atom 1 as Atom 2 is moved in the [0 0 1] plane, calculated via DFT force constants. The potential force surfaces calculated via the radial potential and DFT force constants clearly exhibit different shapes, as the radial potential is forced to have zero force along the arc of equilibrium distance, therefore no parameterization of the radial potential will result in a PES that matches that of DFT.

inclusion of interactions from distant atoms. For example, c-Si requires interactions out to the 8th NN shell, which contains 98 neighbors, for the dispersion to converge [41]. Evaluating this many interactions for a complicated many-body potential would be very expensive. However, the key point here, which can be exploited for speed and reduced computational expense, is that such long ranged interactions are only needed for the harmonic portion of the potential, which can be written in terms of atom pairs. The anharmonic portion of the PES, on the other hand, usually only needs to include 2nd or 3rd NN shells, which contain much fewer atoms. This then naturally leads to using a separable approach to describe the PES, which we describe herein.

2. The failure of traditional potentials.

To clearly delineate what is meant by the harmonic and anharmonic parts of the PES, we first Taylor expand the system's potential energy E about the equilibrium atomic displacements, u_i^α for each atom i and Cartesian direction α, to yield what we will term herein, the Taylor expansion potential (TEP),

$$E = \sum_{ij} \sum_{\alpha\beta} \Phi_{ij}^{\alpha\beta} u_i^\alpha u_j^\beta + \sum_{ijk} \sum_{\alpha\beta\gamma} \Psi_{ijk}^{\alpha\beta\gamma} u_i^\alpha u_j^\beta u_k^\gamma + \dots \qquad (1)$$

where the constants $\Phi_{ij}^{\alpha\beta} = \partial^2 E / \partial u_i^\alpha \partial u_j^\beta$ are the 2nd order interatomic force constants (IFC2s) responsible for what we term "harmonic" aspects of the PES. All higher order terms, starting with $\Psi_{ijk}^{\alpha\beta\gamma} = \partial^3 E / \partial u_i^\alpha \partial u_j^\beta \partial u_k^\gamma$, which are the 3rd order interatomic force constants (IFC3s), account for the anharmonicity in the PES. Obtaining the IFCs by fitting the TEP to DFT has been known to result in a TEP that accurately predicts forces [39], harmonic properties such as mode frequencies [50], and anharmonic properties arising from mode-mode interactions. [51] Thus, the TEP functional form is the IAP that in principle solves the problem at hand, since it evaluates very fast. However, there is an important problem that arises when attempting to use the TEP to run a MD simulation, namely stability.

Here, in using the term "stability", what is meant is the ability for the energy in a MD simulation to be conserved, and for the dynamics to give rise to stable vibrations of the atoms around their equilibrium sites when simulating at a temperature below the material's melting/sublimation/decomposition temperature. When IAPs such as the TEP exhibit instability, it is often the case that the energy is not properly conserved in a microcanonical ensemble, and the temperature quickly rises causing the atoms to deviate far from their equilibrium sites, often flying apart in space – effectively turning into a gas. For example,

Murakami *et al.* showed that the anharmonic TEP yields accurate thermal conductivity in MD simulations, but also noted that dynamical instability of the TEP prohibited simulations at high temperatures [52]. This issue of instability when using the TEP to perform MD simulations has been noted in several reports in the literature, [50,52,53] but it has not been clear why this problem arises.

To realize the methodological advance we present herein, we must first appreciate why traditional IAPs are often so inaccurate. Upon inspection of the long ranged IFC2s for an example material such as c-Si, it was realized that there is an inherent limitation in modelling long-range interatomic interactions [54], when using only the radial distance between pairs of atoms as a geometrical descriptor, as traditional long-range IAPs do. It should be noted that the exclusive usage of radial descriptors, namely the radial distance r_{ij} between two different atoms label i and j, is the most commonly employed descriptor for IAPs (e.g., Lennard-Jones, Coulomb, Morse, etc.). Furthermore, it is the usage of this simple descriptor that enables such potentials to be evaluated quickly, even for long ranged interactions. It has been long recognized that purely radial descriptions are incapable of stabilizing many materials, such as covalently bonded semiconductors, and this is what prompted the invention of more complex IAPs with 3-body interactions that utilize the angles between three atoms θ_{ijk} as a supplementary descriptor. However, the computational expense associated with including 3-body interactions is substantial and as a result, such IAPs are often truncated to only describe 1st or 2nd NN. This is because extending a 3-body potential to include interactions out to 8th NN, for example, would become cost prohibitive, and as a result, long ranged interactions in IAPs typically only employ one of the faster r_{ij} pair-based functional forms previously mentioned.

The central issue is that a using a purely radial descriptor for long ranged interactions does not provide enough flexibility to describe unique and uncoupled IFC2s in all three Cartesian directions. This is because the IFC2s of a radial potential are all coupled via the radial coordinate, resulting in an implicit assumption of radial symmetry in the interatomic forces, as is conceptually illustrated in Fig. 2. It is also important to note that this limitation exists regardless of the parameterization and is therefore intrinsic to the functional form itself; i.e., radial potentials cannot properly capture the forces and IFCs, especially in covalent solids [38]; a mathematical proof of this limitation is given in the SI.

This limitation was also previously realized [41] by exhaustive genetic algorithm searches for parameterizing conventional IAPs to match IFC2s; despite the low error in forces between IAPs and DFT, no IAPs

were able to accurately reproduce the vibrational frequencies. These previous attempts to fit traditional IAPs to long-range IFC2s involved parameterizing long-range interactions that scale exclusively with the interatomic radial distance r, such as r^{-1}, r^{-6}, and r^{-8} for the Coulomb [55], van der Waals [56], and Born [57] potentials, respectively; it was identified that the long-range IFC2s could not be reproduced regardless of parameterization using these radial IAPs [41].

As compared to purely radial descriptions, the harmonic part of the TEP in Equation (1) possesses all of the flexibility needed for capturing the IFC2s, because its parameters are the IFC2s themselves. The problem, however, is with its instability when running MD simulations. [50,52,58] Upon further examination of the TEP functional form itself, it was realized that, apart from usage of a special set of IFC2s that can satisfy the acoustic sum rule, it is in general a translationally variant functional form. It is known that an IAP must exhibit translational invariance in order for it to conserve energy [59], and thus it was suspected that the origin of the instability with the TEP was due to the fact that it is written in a way that references a fixed point in space (i.e., the equilibrium site for each atom). Thus, from a conceptual standpoint, if one were to translate an entire crystal, none of the relative positions between the atoms would change, so there shouldn't be any increase in energy in the system or forces. However, with the TEP, there will be an increase in energy and a restoring force back to the reference locations in the system, since it references a fixed point in space for every atom. There is nonetheless an exception to this, which is if the IFC2s are chosen in such a way that all terms would cancel upon a translation, thereby keeping the total energy fixed, regardless of a translation. This exception is most often referred to as the need to satisfy the *"acoustic sum rule"* [60]. However, we have found that it only seems to solve the instability issue if it is exactly satisfied (i.e., the residual of the acoustic sum must be extremely small – e.g., near machine precision).

In light of this issue, we implemented a more robust solution, which is to instead rewrite the 2nd order term in the TEP in terms of the relative coordinates between the atoms, describing atomic geometry with relative displacements $u_{ij}^\alpha = u_i^\alpha - u_j^\alpha$ instead. In doing so, the *"self-interaction"* term goes away, and the energy only deviates from its minimum value when there is a relative motion between atoms. In this way the functional form itself now exhibits translational invariance by construction. This is important because this translationally invariant form of the TEP (i.e., henceforth referred to as TITEP) is intrinsically stable and can result in stable MD, even if the acoustic sum rule is not strictly satisfied. Thus, it is preferred because it provides more flexible options for how one can model the anharmonicity.

Using TITEP then solves the problem of correctly describing the harmonic portion of the PES in a way that is computationally inexpensive i.e., on the order of Tersoff, even when interactions extend out to 8th neighbors. The remaining challenge is then describing the anharmonicity, as the number of unique IFC3s can outweigh the number of IFC2s, thus requiring a more elaborate/complex description as compared to the harmonic PES. For example, in c-Si the number of unique IFC2s (8th neighbor cutoff) and IFC3s (2nd neighbor cutoff) are 32 and 36 respectively, but for wurtzite GaN they are 237 (4th neighbor cutoff) and 804 (2nd neighbor cutoff) respectively. Thus, it can be challenging to reproduce all the IFC3s with traditional IAPs that have far fewer free parameters than there are unique IFC3s. This then led to the second important insight and central advance of this work, namely we hypothesized that to correctly reproduce a property such as thermal conductivity, there is a subset of IFC3s that are most important to get correct – namely the largest IFC3s are the most important, as will be later shown when applying our method to GaN. This hypothesis was sparked by the prior work [41], which showed that traditional short-range IAPs can reproduce IFC3s with enough accuracy to predict thermal conductivity within 10% error of DFT. We therefore opted to represent the anharmonic parts of the PES utilizing a relatively short-range (e.g., truncated to 2nd nearest neighbors) IAP to capture the anharmonic IFCs, in combination with TITEP to represent the 2nd order

IFCs for longer ranged interactions. Such a potential takes the form,

$$E = \sum_{ij} \sum_{\alpha\beta} \phi_{ij}^{\alpha\beta} u_{ij}^\alpha u_{ij}^\beta + E_{anharmonic} \tag{2}$$

where the first term on the right side is the TITEP with new IFCs $\phi_{ij}^{\alpha\beta}$ related to the TEP IFCs by $\Phi_{ij}^{\alpha\beta} = -\phi_{ij}^{\alpha\beta}$ and $E_{anharmonic}$ is a short-range analytical anharmonic potential. The anharmonic part of Equation (2) may take any form (e.g., Morse, neural network potentials, etc.). We note that one may also write higher order terms of the TEP in a translationally invariant form. However, instability issues may still arise since the divergence to negative infinity of the 3rd order potential energy surface has been suspected as another cause of stability [52], and it is difficult to obtain higher order force constants [58]. since unlike the 2nd order constants, there is no simple or obvious mathematical relation between them and their translationally variant counterparts.

The potential in Equation (2) relieves the difficulties associated with using a single complex IAP with many-body descriptors to capture both the harmonic and anharmonic aspects of the PES out to a large cut-off. This approach instead allows the harmonic TITEP to focus on the predominant harmonic force contributions that often extend beyond 5th nearest neighbors, while the anharmonic terms focus solely on reproducing the short ranged more complex interactions. One could simply use an anharmonic TEP in place of $E_{anharmonic}$, but as previously noted, there are issues with stability and there is also a daunting fitting problem of obtaining all the unique anharmonic IFCs required for simultaneous stability and accuracy [52]. Recent work in compressed sensing [58] seeks to alleviate this issue, but our approach of using a general analytic or machine learned form of $E_{anharmonic}$ is potentially a simpler alternative or something that can be used in conjunction with compressed sensing. It should be noted that the addition of $E_{anharmonic}$ can in general also change the harmonic contributions to the force. Therefore, one must modify the TITEP IFC2s in Equation (2) so that the addition of $E_{anharmonic}$ IFC2s and TITEP IFC2s yields the correct total IFC2s, noting that IFCs are additive (Note: a more detailed description of this procedure is described in the Methods section). Another advantage of this approach lies in the fact that $E_{anharmonic}$ is often an infinitely differentiable function (e.g. some empirical or machine learned potential), and thus maintains the possibility of describing anharmonicity to full order.

3. Application of the new method: The example of crystalline silicon.

To test the aforementioned approach, we applied the functional form in Equation (2), first to c-Si. Previous work [41] found that a simple Morse + 3-body angle potential is enough for accurately modelling anharmonicity in c-Si. Therefore, $E_{anharmonic}$ was chosen to be a Morse + 3-body angle potential of the form

$$E_{anharmonic} = \sum_{ij} D_{ij} [1 - e^{-\alpha_{ij}(r_{ij} - r_{ij}^0)}]^2 + \sum_{a=2}^A \sum_{ijk} k_{a,ijk} (\theta_{ijk} - \theta_{ijk}^0)^a \tag{3}$$

where D_{ij} and α_{ij} are Morse fitting parameters for the ij pair with equilibrium bond length r_{ij}^0, $k_{a,ijk}$ is a fitting parameter for the ijk triplet with equilibrium angle θ_{ijk}^0 and angle expansion exponent a, where the number of terms A in the angle expansion is chosen by the user. It is important to note here that we define unique interactions in the sum of Equation (3) for every pair or triplet, thus increasing the flexibility of this anharmonic potential. We also take advantage of structural symmetry by declaring identical distances or angles between identical types of atoms to be governed by the same potential parameters. Equation (3) was chosen to have a cutoff out to 2nd NN since anharmonic interactions out to 2nd NN are important for predicting thermal conductivity in c-Si [39]. The angular expansion in one of our potentials went out to $A = 2$, and is termed the Morse + 3-body harmonic (M3H) potential,

Table 1

Force, IFC2, and IFC3 MPE and WMPE for 10 commonly cited potentials in literature compared to the potentials developed in this work.

	Tersoff 1988 [28]	Tersoff 1989 [29]	Tersoff 1990 [30]	Tersoff 2007 [32]	SW [31]	SW 2012 [33]	EDIP 1998 [34]	EDIP 2012 [35]	REAX [36]	GAP [37]	TITEP + M3H	TITEP + M3A
Force MPE	24.1	18.8	18.9	18.8	36.5	13.4	52.1	48.6	46.1	5.9	2.94	2.88
IFC2 MPE	91.2	88.8	76.5	90.8	87.9	83.3	83.9	86.3	85.1	99.6	39.9	10.5
IFC2 WMPE	1.4	1.4	1.4	1.4	3.6	0.46	5.7	5.1	4.9	0.19	0.048	4.4E-3
IFC3 MPE	130.7	338.7	400.1	335.5	210.9	202.1	358.9	391.8	176.9	805.2	80.3	64.2
IFC3 WMPE	10.7	11.7	12.5	11.6	10.3	10.9	32.9	57.1	6.8	24.0	0.32	0.29

while the other potential included more anharmonicity out to $A = 4$, and was termed the M3A potential. The TEP + M3H and TEP + M3A potentials were then parameterized with the POPS program [41] (i.e., using a genetic algorithm) to match DFT forces, IFC2s, and IFC3s. More details pertaining to the fitting procedure and DFT details are provided in the Methods section. The total force, IFC2, and IFC3 mean percent errors (MPE) and weighted mean percent errors (WMPE) of the resulting IAPs are compared to 10 commonly cited potentials in literature and are shown in Table 1 (note: the definition of errors is given in the SI).

The spread of force errors in Table 1, ranges from about 3% to 50%. Force errors of 50% have been shown to drastically differ in magnitude and direction for any given snapshot of DFT calculated forces [41]. The TITEP + M3H and TITEP + M3A IAPs outperform all other IAPs but are only marginally better than GAP at reproducing the forces. This is not surprising, since GAP has been shown to be a flexible functional form capable of describing many situations and was trained to hundreds of thousands of forces [37]. By training machine learned IAPs like GAP only to the total forces, however, these IAPs fail to capture smaller anharmonic components of the forces, which may only comprise < 10% of the total force in materials like c-Si, but are much more sensitive and important for describing thermal conductivity. For IFC2 errors, our TITEP + M3H and TITEP + M3A may seem high despite using a supposedly exact description of the harmonic PES, the TITEP, but the definition of mean percent error here causes the error to diverge if small IFCs are not well described. We therefore use the WMPE to show that our potentials perform much better at reproducing the large IFCs compared to traditional potentials, and we will show that large IFC3s may be most important in describing thermal transport in the next section. The results for these TITEP + M3H and TITEP + M3A IAPs in terms of phonon dispersion and thermal conductivity is shown in Fig. 3.

To the best of our knowledge, this level of agreement, with a 1% thermal conductivity error from 100 K to 1000 K and near exact phonon frequency predictions, has never been achieved before with an IAP for c-Si. Furthermore, the computational cost of these new c-Si potentials are on the order of traditional potentials like Tersoff (see the SI for details), which is their major advantage over a machine learned potential like GAP.

Despite its simplicity, the anharmonic potential of Equation (3) works well for c-Si since this system contains only 32 unique IFC3s, and the Morse + 3-body angle potential out to 2nd neighbors contained 30 fitting parameters; reproduction of the IFC3s was therefore manageable in terms of the number of unknowns and fitting parameters. More complex materials with less symmetry in the lattice, however, contain more IFC3s and therefore require more flexibility and fitting parameters for the description of anharmonicity. Equation (3) therefore fails to capture anharmonicity in materials with more complex structure, such as wurtzite GaN, which has 804 unique IFC3s. As a result, no accurate IAP has ever been made for thermal transport in GaN, despite its great technological importance, and the preeminence of the thermal bottleneck in wide band gap electronics.

4. Modeling thermal vibrations in wurtzite GaN

Wurtzite GaN, with 804 IFC3s, requires more flexibility to describe

the anharmonicity than Equation (3) can offer. We confirmed this with exhaustive genetic algorithm fits of a Morse + 3-body potential out to 2nd nearest neighbors, containing 136 fitting parameters, and the IFC3s could not be matched. Our alternative solution for this situation was to use a more flexible machine learned spectral neighbor analysis potential (SNAP) [61] to describe only the anharmonic part of the force, while the TITEP describes the known harmonic part. Here, it is important to emphasize that we trained SNAP only to the anharmonic part of the force, obtained by subtracting the harmonic force from the total force. This restricts SNAP to only needing a cut-off out to 2nd NN, the cutoff required to capture the relevant IFC3s for thermal transport in GaN, as opposed to a long-ranged version (i.e., 8th NN), if SNAP were to be used to capture the harmonic forces as well. This is important because it keeps the computational cost low, as an 8th nearest neighbor SNAP potential for c-Si would be 4 orders of magnitude slower than traditional IAPs like Tersoff, as shown in Fig. 4.

Conversely, a 2nd NN SNAP IAP is only 2 orders of magnitude slower than Tersoff. Thus, the usage of TITEP + 2nd NN SNAP preserves accuracy with respect to the dispersion yet saves 2 orders of magnitude in computational cost compared to a longer ranged SNAP.

For GaN, the total potential energy is still given by Equation (2), except that the anharmonic potential is replaced by SNAP with 56 fitting parameters for each atomic species (gallium and nitrogen). Training this potential to 71 GaN configurations resulted in a 7% force error for GaN. Most of this force agreement comes from harmonic forces, resulting in excellent phonon dispersion calculations shown in Fig. 5. We note here that our DFT results fail to exactly match experimental values, and we attribute this to the fact that polar materials like GaN require ad-hoc corrections to dispersion via Born effective charges [62]. While the DFT training set may always be optimized further, the focus here is to show that the phonon potential exactly reproduces the DFT phonon dispersion.

In addition to this excellent agreement with *ab initio* harmonic behavior, our GaN IAP also reproduces the anharmonic interactions decently. This is exhibited by the < ~ 15% thermal conductivity error across a wide range of temperatures, in both in-plane (perpendicular to the c-axis) and cross-plane (parallel to c-axis) directions, as shown in Fig. 6.

These thermal conductivity results verify that the SNAP anharmonic potential provides reasonable agreement with the *ab initio* description of the anharmonic PES, particularly whatever is necessary to describe thermal conductivity.

Some disagreement in thermal conductivity seems reasonable for this situation, since our anharmonic SNAP potential contained only 112 fitting parameters, while there are 950 unique IFC3s for this system out to 2nd nearest neighbors. We therefore cannot expect to capture all IFC3s exactly, and indeed the total IFC3 MPE was 45%, and the weighted MPE was 9.6%. Fig. 7 shows the direct comparison between the IAP and DFT IFC3s. Our 112 parameter SNAP captured the top 10% largest IFC3s i.e., by magnitude, to within 10% error. What is also shown in Fig. 7, are plots of the percent error for each IFC3 as a function of its reference DFT magnitude.

Fig. 7 shows that our IAP captures the top 10% largest IFC3s with ~ 10% error, and the general trend is that smaller IFC3s are more difficult to capture. This is because the training procedure for the
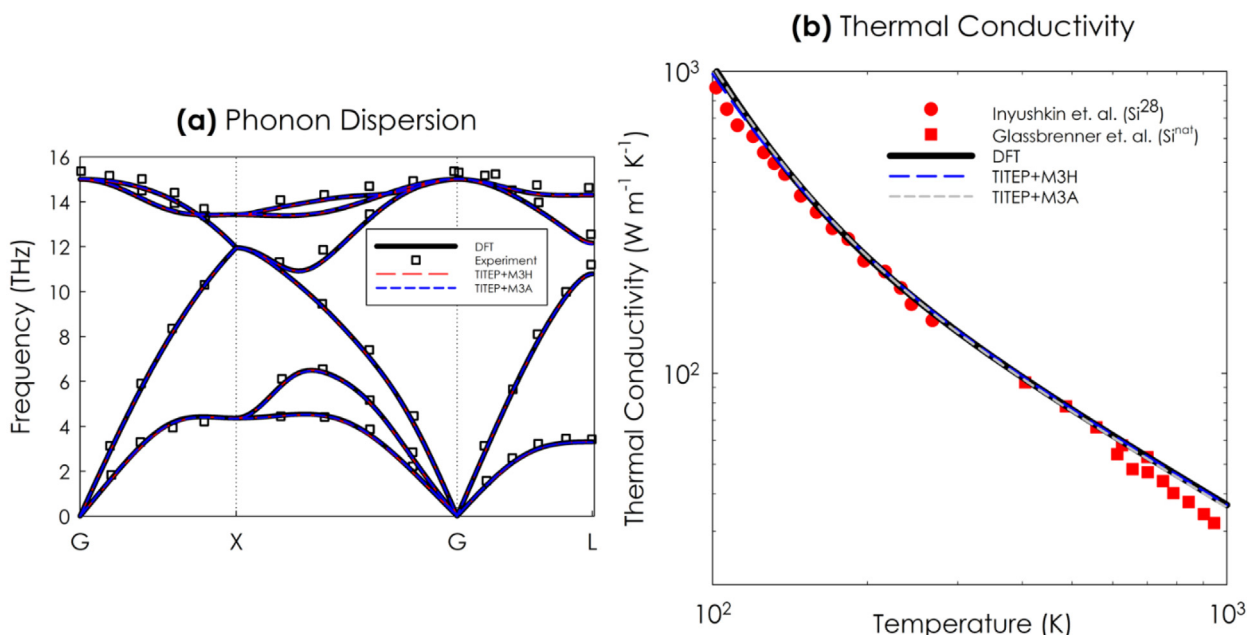
Fig. 3. (a) Phonon dispersion curves and (b) BTE relaxation time approximation (RTA) thermal conductivity calculation using the long-range TITEP combined with short-range Morse + 3-body angular potentials (dashed lines) compared to DFT (black line) and neutron scattering experiments [38] (squares) and thermal conductivity measurements (circles and squares).
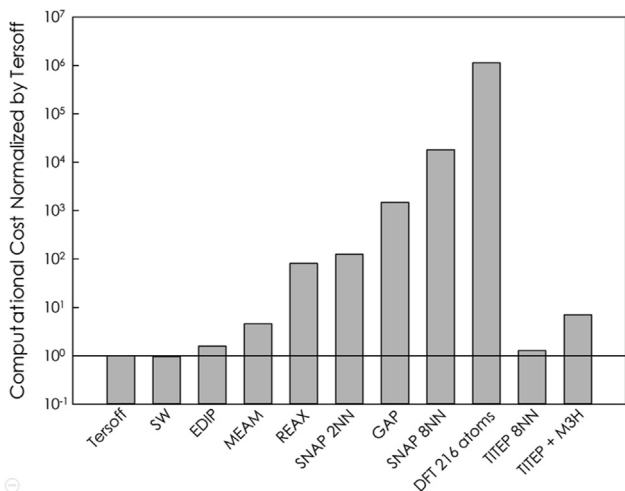

Fig. 4. Computational expense (seconds per timestep per atom per core) for a variety of potentials and DFT, normalized by Tersoff. For our c-Si potential, TITEP + M3H, we show only an order of magnitude increase in cost compared to Tersoff, which is still orders of magnitude lower than other modern potentials, but unparalleled accuracy in modelling harmonic and anharmonic vibrations.

Fig. 5. GaN phonon dispersion calculations using the SNAP + TITEP potential (red line) compared to DFT (black line), experiments [63], and Tersoff [64] and SW [65] potentials from literature. (For interpretation of the references to colour in this figure legend, the reader is referred to the web version of this article.)

anharmonic SNAP potential includes only total anharmonic forces, and thus it is biased towards reproducing the largest contributions to the anharmonic forces. As a result, the training procedure knows virtually nothing about the smaller components of these forces, which arise from the smaller IFC3s. The level of IFC3 agreement we obtained seems sufficient for modelling thermal conductivity within 15%, and this could presumably be improved if the IFC3s were explicitly included in the SNAP fitting process. Nonetheless, these results suggest that the largest IFC3s are most important for predicting thermal transport. These results furthermore show that the general functional form of Equation (2) can accurately describe thermal vibrations/normal modes and their interactions which result in thermal conductivity, provided that the anharmonic portion possesses enough flexibility to capture the anharmonicity, whose complexity is determined by the number of
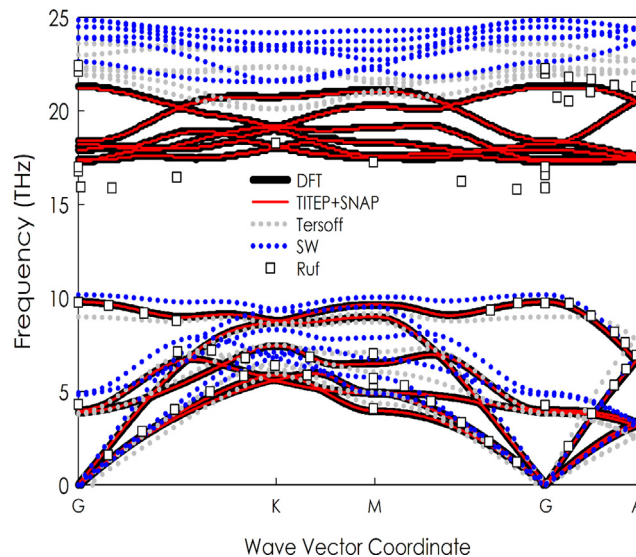
unique anharmonic IFCs. We note that the general form of $E_{anharmonic}$ in Equation (2) is often infinitely differentiable and therefore contains all orders of anharmonicity, representing another advantage over the traditional anharmonic TEP, although the accuracy for higher order anharmonicity with our method will be investigated in future work.

5. Conclusions

To summarize, we showed the utility of designing IAPs according to Equation (2), where separate functional forms are used to describe the harmonic and anharmonic parts of the PES. This separation is useful because the number of atoms (i.e., the length of the cut-off) and
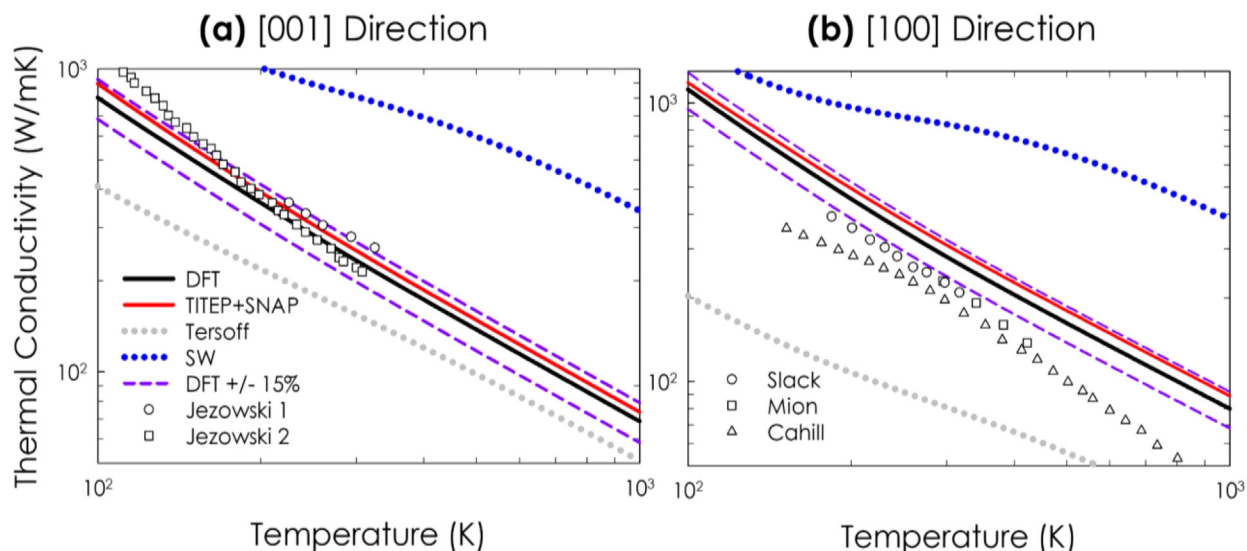
Fig. 6. (a) GaN BTE RTA in-plane thermal conductivity calculations using our TITEP + SNAP potential (red line) compared to DFT calculations (black line), experiments [66,67], and Tersoff [64] (grey dots) and SW [65] (blue dots) potentials from literature. The purple dashed lines are 15% error bars on DFT thermal conductivity. (b) GaN BTE RTA cross-plane (parallel to *c*-axis) thermal conductivity calculations using our TITEP + SNAP potential (red line) compared to DFT calculations (black line), experiments [68–70], and potentials from literature. (For interpretation of the references to colour in this figure legend, the reader is referred to the web version of this article.)

necessary complexity differs significantly for each portion of the PES. The harmonic portion can be exactly captured by a simple form, referred to herein as the TITEP, which solves the stability issue by rewriting the IAP in a form where it is intrinsically translationally invariant – regardless of parameterization. The use of TITEP solves the problem of correctly describing the long-ranged interactions, and does so with minimal computational expense, which is a major advantage over using orders of magnitude more expensive and complex many-body potentials to achieve the same level of accuracy. The separation also allows an anharmonic potential to focus on the anharmonicity, which is often difficult and complex for a single potential to capture when training to the total force since the harmonic contributions dominate the force magnitude. Consequently, the methodology presented yields accurate IAPs that can be used for describing atomic vibrations and performing stable MD simulations of c-Si and GaN, which are two highly important and technologically relevant materials.

This new approach sets a new foundation upon which IAPs that deal with more complex atomic environments can be built upon, such as systems with defects, amorphous materials, interfaces, dopants, alloys and nanostructures. For these more complex systems, each atom's IFC2 may be stored in memory for use in the TITEP, while a flexible machined learned IAP such as SNAP can describe the anharmonicity in a general and more easily transferable way. Using this method, the functional form of Equation (2) is currently the most suitable for modelling atomic vibrations and thermal transport with unparalleled accuracy and computational speed. With this foundation, other phenomena (e.g., chemical reactions, [8] mass/ion diffusion [9], and phase changes[10]) that depend on or involve thermal vibrations can now be described more accurately with predictive power.
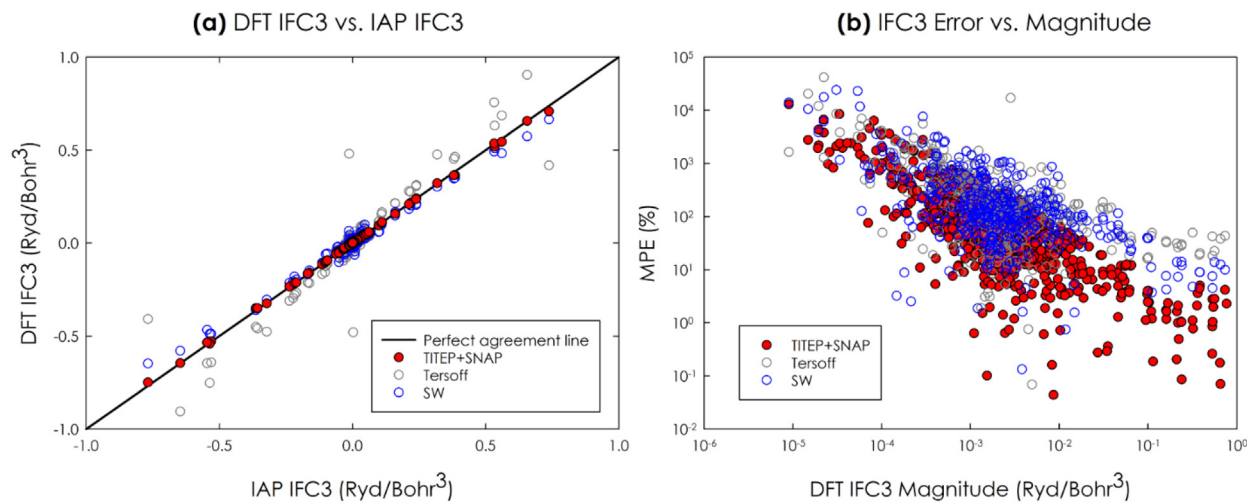

Fig. 7. (a) Comparison between DFT IFC3 values and IAP IFC3 values for our TITEP + SNAP potential compared to Tersoff [64] (grey circles) and SW [65] (blue circles) potentials from literature. (b) Percent error of IFC3s by magnitude for wurtzite GaN. The bottom axis represents magnitude of DFT IFC3s, while the top axis is the percent error between the IAP IFC3 and the DFT IFC3. (For interpretation of the references to colour in this figure legend, the reader is referred to the web version of this article.)

6. Methods

Our methods of parameterizing IAPs using the general functional form in Equation (2) is presented herein. We used to methods in this paper – the first method, for c-Si, involves fitting $E_{anharmonic}$ in Equation (2) to the total DFT forces and/or force constants (we fit to 2nd and 3rd order force constants for c-Si), then adding a corrected harmonic Taylor expansion on top of this potential. The second method, used for GaN, involves fitting $E_{anharmonic}$ to the anharmonic DFT forces obtained by subtracting the harmonic forces. The first method (for c-Si) is described as follows:

1. Perform DFT calculations to obtain training data in the form of forces on atoms, across many configurations.
2. Fit an anharmonic potential $E_{anharmonic}$ to the total DFT forces and/or force constants (Note: We used 2nd and 3rd order force constants in making the c-Si potential).
3. The fitted anharmonic potential will contain some errors in 2nd order force constants; calculate the $E_{anharmonic}$ IFC2s, $\Phi^{anharmonic}$, and obtain the corrected IFC2s $\Phi^{corrected} = \Phi^{DFT} - \Phi^{anharmonic}$.
4. Use $\Phi^{corrected}$ for the IFC2s in the functional form of Equation (2).

The second method, that we used for GaN (that you read in the Methods section), was as follows:

1. Perform DFT calculations to obtain training data in the form of forces on atoms, across many configurations.
2. Fit a 2nd order TEP to obtain the DFT IFC2s, Φ^{DFT}.
3. Calculate the anharmonic DFT forces by subtracting the harmonic force, calculated with the IFC2s obtained in Step 2, from the total DFT force.
4. Fit the anharmonic potential $E_{anharmonic}$ to the anharmonic forces obtained in Step 3.
5. The fitted anharmonic potential may still have its own IFC2s due to the unavoidable harmonic curvature of many potentials (e.g., the built-in well of the Morse potential). Calculate the $E_{anharmonic}$ IFC2s, $\Phi^{anharmonic}$, and obtain the corrected IFC2s $\Phi^{corrected} = \Phi^{DFT} - \Phi^{anharmonic}$.
6. Use $\Phi^{corrected}$ for the IFC2s in the functional form of Equation (2).

Obtaining the harmonic IFC2s in all scenarios was achieved by fitting a harmonic TEP to the forces calculated from a potential or DFT, using the least squares optimization procedure in the Alamode program [39]. Parameterizing the anharmonic potential was performed with the POPs [41] program in the case of the Morse and 3-body potentials for c-Si. For the GaN SNAP potential, we performed least squares fitting to train SNAP against DFT forces, as described in literature [61]. We should note that when obtaining the 2nd order IFCs, there will be some implicit temperature dependence since they are obtained via displacing atoms. This does not seem to affect agreement with DFT dispersion curves, but the temperature effect on IFCs should be noted [50]; one may remedy this issue by using a lookup table in the potential associating a given set of IFCs for a particular temperature in a MD simulation, for example. In the first method (for c-Si), the anharmonic IFCs were obtained by fitting force–displacement data from the potential to a TEP via the Alamode program [39]. All other anharmonic IFCs in this paper, such as Fig. 7, were also obtained via fitting a TEP to force–displacement data from the potential.

7. Author information

Andrew Rohskopf developed the interatomic potential fitting codes used in this work and began the concept of decomposing forces into harmonic and anharmonic components regarding fitting potentials. Spencer Wyant and Kiarash Gordiz helped with testing and validation of the current method, while Hamid Reza Seyf and Murali Gopal Muraleedharan helped with testing and validation of the potential fitting code. Asegun Henry served as an advisor on this project, offering useful insight.

CRediT authorship contribution statement

Andrew Rohskopf: Conceptualization, Methodology, Visualization, Writing - original draft. **Spencer Wyant:** Validation, Data curation, Writing - original draft. **Kiarash Gordiz:** Validation, Data curation, Writing - original draft. **Hamid Reza Seyf:** Investigation. **Murali Gopal Muraleedharan:** Investigation. **Asegun Henry:** Supervision, Writing - review & editing.

Data availability

The LAMMPS input scripts for the interatomic potentials, along with LAMMPS pair style codes for the custom-made potentials, are included as extra files with the manuscript. The code used for fitting potentials is available open-source at https://github.com/rohskopf/pops.

Appendix A. Supplementary data

Supplementary data to this article can be found online at https://doi.org/10.1016/j.commatsci.2020.109884.

References

[1] R. Costescu, D. Cahill, F. Fabreguette, Z. Sechrist, S.J.J.A.P. George, Ultra-Low Thermal Conductivity in W/Al, J. Appl. Phys. 81 (1997) 6692.
[2] S.-M. Lee, D.G. Cahill, R.J.A.p. Venkatasubramanian, et al., Thermal conductivity of Si–Ge superlattices, Appl. Phys. Lett. 70 (1997) 2957–2959.
[3] M.C. Wingert, et al., Sub-amorphous thermal conductivity in ultrathin crystalline silicon nanotubes, Nano Lett. 15 (2015) 2605–2611.
[4] C. Chiritescu, et al., Ultralow thermal conductivity in disordered, layered WSe2 crystals, Science 315 (2007) 351–353.
[5] C. Chiritescu, et al., Low thermal conductivity in nanoscale layered materials synthesized by the method of modulated elemental reactants, J. Appl. Phys. 104 (2008) 33533.
[6] D.G. Cahill, S.K. Watson, R.O.J.P.R.B. Pohl, Lower limit to the thermal conductivity of disordered crystals, Phys. Rev. B 46 (1992) 6131.
[7] M.D. Losego, I.P. Blitz, R.A. Vaia, D.G. Cahill, P.V. Braun, Ultralow thermal conductivity in organoclay nanolaminates synthesized via simple self-assembly, Nano Lett. 13 (2013) 2215–2219, https://doi.org/10.1021/nl4007326.
[8] K. Kim, M.J.A.A. Kaviany, Phonocatalysis. An ab initio simulation experiment, AIP Adv. 6 (2016) 65124.
[9] M. Ma, et al., Water transport inside carbon nanotubes mediated by phonon-induced oscillating friction, Nat. Nanotechnol. 10 (2015) 692.
[10] M. Rini, et al., Control of the electronic phase of a manganite by mode-selective vibrational excitation, Nature 449 (2007) 72.
[11] M. Forst, R. Mankowsky, A.J.A. Cavalleri, o. c. r. Mode-selective control of the crystal lattice, Acc. Chem. Res. 48 (2015) 380–387.
[12] J.C.J.S. Tully, Mode-selective control of surface reactions, Science 312 (2006) 1004–1005.
[13] Z. Liu, L.C. Feldman, N. Tolk, Z. Zhang, P.I.J.S. Cohen, Desorption of H from Si (111) by resonant excitation of the Si-H vibrational stretch mode, Science 312 (2006) 1024–1026.
[14] A. Sinha, M.C. Hsiao, F.F.J.T.J.o.C.P. Crim, Bond-selected bimolecular chemistry: H + HOD (4νOH)→ OD + H2, J. Chem. Phys. 92 (1990) 6333–6335.
[15] M.J. Bronikowski, W.R. Simpson, R.N.J.T.J.o.P.C. Zare, Effect of reagent vibration on the hydrogen atom + water-d reaction: an example of bond-specific chemistry, J. Phys. Chem. 97 (1993) 2194–2203.
[16] I. Hussla, et al., Infrared-laser-induced photodesorption of NH 3 and ND 3 adsorbed on single-crystal Cu (100) and Ag film, Phys. Rev. B 32 (1985) 3489.

[17] J.I. Pascual, N. Lorente, Z. Song, H. Conrad, H.-P.J.N. Rust, Selectivity in vibrationally mediated single-molecule chemistry, Nature 423 (2003) 525.

[18] W. Lv, et al., Direct calculation of modal contributions to thermal conductivity via Green–Kubo modal analysis, New J. Phys. 18 (1) (2016).

[19] K. Gordiz, et al., A formalism for calculating the modal contributions to thermal interface conductance, New J. Phys. 17 (10) (2015).

[20] K. Kadau, T.C. Germann, P.S.J.I.J.o.M.P.C. Lomdahl, Molecular dynamics comes of age: 320 billion atom simulation on BlueGene/L, Int. J. Mod. Phys. C 17 (2006) 1755–1761.

[21] R.A. Böckmann, H.J.N.S. Grubmüller, M. Biology, Nanoseconds molecular dynamics simulation of primary mechanical energy transfer steps in F 1-ATP synthase, Nat. Struct. Biol. 9 (2002) 198.

[22] D. Rodney, G.J.P.R.B. Martin, Dislocation pinning by glissile interstitial loops in a nickel crystal: A molecular-dynamics study, Phys. Rev. B 61 (2000) 8714.

[23] A.N. Andriotis, M. Menon, G.J.P. Froudakis, r. l. Catalytic action of Ni atoms in the formation of carbon nanotubes: a molecular dynamics study, Phys. Rev. Lett. 85 (2000) 3193.

[24] D. Voneshen, H. Walker, K. Refson, J.J.P. Goff, r. l. Hopping time scales and the phonon-liquid electron-crystal picture in thermoelectric copper selenide, Phys. Rev. Lett. 118 (2017) 145901.

[25] S. Gnanakaran, H. Nymeyer, J. Portman, K.Y. Sanbonmatsu, A.E.J.C. Garcıa, o. i. s. b. Peptide folding simulations, Curr. Opin. Struct. Biol. 13 (2003) 168–174.

[26] Z. Qin, X.-Q. Feng, J. Zou, Y. Yin, S.-W.J.A.P.L. Yu, Superior flexibility of super carbon nanotubes: Molecular dynamics simulations, Appl. Phys. Lett. 91 (2007) 043108.

[27] J.-W. Jiang, J.-S. Wang, B.J.P.R.B. Li, Young's modulus of graphene: a molecular dynamics study, Phys. Rev. B 80 (2009) 113405.

[28] J.J.P.R.B. Tersoff, Empirical interatomic potential for silicon with improved elastic properties, Phys. Rev. B 38 (1988) 9902.

[29] J J.P.R.B. Tersoff, Modeling solid-state chemistry: Interatomic potentials for multicomponent systems, Phys. Rev. B 39 (1989) 5566.

[30] J.J.P.r. Tersoff, et al., Carbon defects and defect reactions in silicon, Phys. Rev. Lett. 64 (1990) 1757.

[31] F.H. Stillinger, T.A.J.P.r.B. Weber, Computer simulation of local order in condensed phases of silicon, Phys. Rev. B 31 (1985) 5262.

[32] S. Munetoh, T. Motooka, K. Moriguchi, A.J.C.M.S. Shintani, Interatomic potential for Si–O systems using Tersoff parameterization, Comput. Mater. Sci. 39 (2007) 334–339.

[33] Y. Lee, G.S.J.P.R.B. Hwang, Force-matching-based parameterization of the Stillinger-Weber potential for thermal conduction in silicon, Phys. Rev. B 85 (2012) 125204.

[34] J.F. Justo, M.Z. Bazant, E. Kaxiras, V.V. Bulatov, S.J.P.r.B. Yip, Interatomic potential for silicon defects and disordered phases, Phys. Rev. B 58 (1998) 2539.

[35] C. Jiang, D. Morgan, I.J.P.R.B. Szlufarska, Carbon tri-interstitial defect: A model for the D II center, Phys. Rev. B 86 (2012) 144118.

[36] A.C. Van Duin, et al., ReaxFFSiO reactive force field for silicon and silicon oxide systems, J. Phys. Chem. A 107 (2003) 3803–3811.

[37] A. Bartok, et al., Gaussian Approximation Potentials: The Accuracy of Quantum Mechanics, without the Electrons, Phys. Rev. Lett. 104 (13) (2010) 136403.

[38] W.J.P.R.B. Weber, Adiabatic bond charge model for the phonons in diamond, Si, Ge, and $\alpha-$ Sn, Phys. Rev. B 15 (1977) 4789.

[39] T. Tadano, et al., Anharmonic force constants extracted from first-principles molecular dynamics: applications to heat transfer simulations. J. Phys.: Condens. Matter 26 (22) (2014) 225402.

[40] T. Feng, L. Lindsay, X.J.P.R.B. Ruan, Four-phonon scattering significantly reduces intrinsic thermal conductivity of solids, Phys. Rev. B 96 (2017) 161201.

[41] A. Rohskopf, H.R. Seyf, K. Gordiz, T. Tadano, A.J.N.C.M. Henry, Empirical interatomic potentials optimized for phonon properties, NPJ Comput. Mater. 3 (2017) 27.

[42] E. Minamitani, M. Ogura, S.J.A.P.E. Watanabe, Simulating lattice thermal conductivity in semiconducting materials using high-dimensional neural network potential, Appl. Phys. Express 12 (2019) 095001.

[43] H. Babaei, R. Guo, A. Hashemi, S.J.P.R.M. Lee, Machine-learning-based interatomic potential for phonon transport in perfect crystalline Si and crystalline Si with vacancies, Phys. Rev. Mater. 3 (2019) 074603.

[44] R. Li, E. Lee, T.J.M.T.P. Luo, A unified deep neural network potential capable of predicting thermal conductivity of silicon in different phases, Mater. Today Phys. 100181 (2020).

[45] M.T. Dove, M.T. Dove, Introduction to lattice dynamics, Vol. 4 Cambridge university press, 1993.

[46] T. Smith, G.J.J.o.P.C.S.S.P. White, The low-temperature thermal expansion and Gruneisen parameters of some tetrahedrally bonded solids, Solid State Phys. 8 (1975) 2031.

[47] K. Esfarjani, H.T.J.P.R.B. Stokes, Method to extract anharmonic force constants from first principles calculations, Phys. Rev. B 77 (2008) 144112.

[48] Z. Aksamija, U.J.J.o.C.E. Ravaioli, Joule heating and phonon transport in silicon MOSFETs, J. Comput. Electron. 5 (2006) 431–434.

[49] T. Feurer, J.C. Vaughan, K.A.J.S. Nelson, Spatiotemporal coherent control of lattice vibrational waves, Science 299 (2003) 374–377.

[50] O. Hellman, P. Steneteg, I.A. Abrikosov, S.I.J.P.R.B. Simak, Temperature dependent effective potential method for accurate free energy calculations of solids, Phys. Rev. B 87 (2013) 104111.

[51] A. Togo, I.J.S.M. Tanaka, First principles phonon calculations in materials science, Scr. Mater. 108 (2015) 1–5.

[52] T. Murakami, T. Shiga, T. Hori, K. Esfarjani, J.J.E. Shiomi, Importance of local force fields on lattice thermal conductivity reduction in PbTe1 $-$ xSex alloys, EPL (Europhysics Letters) 102 (2013) 46002.

[53] Z. Tian, et al., Phonon conduction in PbSe, PbTe, and PbTe 1 $-$ x Se x from first-principles calculations, Phys. Rev. B 85 (2012) 184303.

[54] W.J.P.R.L. Weber, New bond-charge model for the lattice dynamics of diamond-type semiconductors, Phys. Rev. Lett. 33 (1974) 371.

[55] C.J. Fennell, J.D.J.T.J. Gezelter, o. c. p. Is the Ewald summation still necessary? Pairwise alternatives to the accepted standard for long-range electrostatics, J. Chem. Phys. 124 (2006) 234104.

[56] H.J.p. Hamaker, The London—van der Waals attraction between spherical particles, Physica 4 (1937) 1058–1072.

[57] M.P. Tosi, Cohesion of ionic solids in the Born model, Solid State Phys. 16 (1964) 1–120.

[58] F. Zhou, W. Nielson, Y. Xia, V.J.a.p.a. Ozolins, Compressive sensing lattice dynamics. I. General formalism, Phys. Rev. B 100 (2018).

[59] A.P. Bartók, R. Kondor, G.J.P.R.B. Csányi, On representing chemical environments, Phys. Rev. B 87 (2013) 184115.

[60] R.M. Pick, M.H. Cohen, R.M.J.P.R.B. Martin, Microscopic theory of force constants in the adiabatic approximation, Phys. Rev. B 1 (1970) 910.

[61] A.P. Thompson, L.P. Swiler, C.R. Trott, S.M. Foiles, G.J.J.J.o.C.P. Tucker, Spectral neighbor analysis method for automated generation of quantum-accurate interatomic potentials, J. Comput. Phys. 285 (2015) 316–330.

[62] X. Gonze, C.J.P.R.B. Lee, Dynamical matrices, Born effective charges, dielectric permittivity tensors, and interatomic force constants from density-functional perturbation theory, Phys. Rev. B 55 (1997) 10355.

[63] T. Ruf, et al., Phonon dispersion curves in wurtzite-structure GaN determined by inelastic x-ray scattering, Phys. Rev. Lett. 86 (2001) 906.

[64] J. Nord, K. Albe, P. Erhart, K.J.J.o.P.C.M. Nordlund, Modelling of compound semiconductors: analytical bond-order potential for gallium, nitrogen and gallium nitride, J. Phys.: Condens. Matter 15 (2003) 5649.

[65] A. Béré, A.J.P.M. Serra, On the atomic structures, mobility and interactions of extended defects in GaN: dislocations, tilt and twin boundaries, Philos. Mag. 86 (2006) 2159–2192.

[66] A. Jeżowski, et al., Thermal conductivity of heavily doped bulk crystals GaN: O. Free carriers contribution, Mater. Res. Express 2 (2015) 085902.

[67] A. Jeżowski, et al., Thermal conductivity of GaN crystals in 4.2–300 K range, Solid State Commun. 128 (2003) 69–73.

[68] C. Mion, J. Muth, E. Preble, D.J.A.P.L. Hanser, Accurate dependence of gallium nitride thermal conductivity on dislocation density, Appl. Phys. Lett. 89 (2006) 92123.

[69] G.A. Slack, L.J. Schowalter, D. Morelli, Freitas, Some effects of oxygen impurities on AlN and GaN, J. Cryst. Growth 246 (2002) 287–298.

[70] Q. Zheng, et al., Thermal conductivity of GaN, GaN 71, and SiC from 150 K to 850 K, Phys. Rev. Mater. 3 (2019) 014601.